Available online at UofKEJ Website Here
UofKEJ Vol. 13 Issue 2 pp. 10-22 (2025)

UNIVERSITY OF KHARTOUM ENGINEERING JOURNAL (UofKEJ)

Modeling Dust Storm Impacts on PV System Performance in Arid Regions: A Case Study of Sudan

Sami M. Sharif[1*]

[1]Department of Electrical and Electronics Engineering, University of Khartoum.
[*]Corresponding author (E-mail: smsharif@uofk.edu)

ARTICLE INFO

Keywords:
Photovoltaic (PV) systems, dust storms, optical depth, attenuation, visibility, extinction coefficient, solar performance.

Article History:
Received on: 24 July 2025
Accepted on:

Article Type:
Research Article

DOI: 10.5332/uofkej.v13i2

ABSTRACT

This study presents a mathematical model to predict the impact of dust storms on solar irradiance and photovoltaic (PV) system performance, with a focus on arid regions like Sudan. Using LiDAR data and locally collected dust samples, the model analyzes the relationship between dust particle-size distribution (PSD), extinction coefficients, and visibility. Results indicate that dust storms significantly increase optical depth and light attenuation, particularly at low sun elevation angles, leading to substantial reductions in solar irradiance. The proposed model incorporates optical and meteorological parameters—such as normalized polarizability, visibility, and particle density—within a semi-analytical framework. Unlike traditional empirical models, this approach integrates region-specific dust properties and particle physics, enhancing predictive accuracy for PV output losses. The model predicts irradiance losses of up to 50% during severe dust events, aligning well with reported field observations from similar environments in the Middle East and North Africa. This work contributes a valuable tool for solar energy forecasting and system planning in dusty regions. It also offers insights into visibility degradation during dust storms, supporting applications in both energy and environmental monitoring.

1. INTRODUCTION

Solar photovoltaic (PV) energy systems have emerged as one of the fastest-growing renewable energy technologies worldwide. Driven by climate concerns and the depletion of fossil fuels, many countries are shifting toward clean energy sources, with PV systems playing a central role. Over the past decade, the cost of PV technology has dropped by more than 90%, making it highly competitive with conventional energy sources such as fossil fuels and wind power. According to IRENA [1], solar PV is expected to supply approximately 25% of global electricity demand by 2050, with an installed capacity exceeding 8,500 GW.

The performance of PV systems is highly dependent on environmental conditions, especially solar irradiance and temperature. Among the key factors affecting solar irradiance are atmospheric aerosols—primarily dust particles—suspended during dust storms. These particles scatter and absorb sunlight, thereby reducing the amount of energy reaching PV panels and lowering system efficiency.

Dust storms are particularly frequent and intense in arid and semi-arid regions such as Sudan, where the dry soil, high wind activity, and lack of vegetation contribute to sustained airborne dust. Compared to other regions like the Gulf or North Africa, Sudan experiences longer-duration storms with coarser dust and higher concentrations near the surface—conditions that are not adequately captured by generalized models developed elsewhere.

Despite the growing adoption of PV systems in Sudan, most existing models predicting dust-related performance losses are overly empirical or based on datasets from different geographic and climatic contexts. These models often lack physical detail and do not incorporate Sudan-specific dust properties or visibility metrics. This paper addresses that gap by developing a region-specific, semi-analytical model that links optical and meteorological parameters to PV performance. The model incorporates real dust data from

Sudan and offers improved accuracy in forecasting solar output during dust events.

2. RELATED WORK

Numerous studies have explored the influence of dust and aerosols on solar radiation and PV system performance, particularly in dust-prone regions such as the Middle East, North Africa, and South Asia. These works can be categorized into three main areas:

A. Empirical and Experimental Studies on Dust Effects on Solar Irradiance

Several studies have quantified the reduction in solar irradiance during dust events using observational data. For example, Papachristopoulou et al. [2] reported that dust aerosols can reduce direct normal irradiance (DNI) by up to 23% and global horizontal irradiance (GHI) by up to 5% during extreme events. Monteiro et al. [3] documented a 90% drop in DNI and a 50% drop in GHI in the Eastern Mediterranean. In Iraq, Chaichan et al. [4] found a 55% reduction in irradiance, while Masoom et al. [5] reported a 40% decline in DNI over three days in India.

B. Radiative Transfer and Optical Modeling

Other studies have focused on modeling the interaction between dust and solar radiation using radiative transfer theory and Mie scattering models. Foundational works by Haywood and Boucher [7], and Balkanski et al. [8] established frameworks for aerosol radiative forcing. Lindberg et al. [9] and Sharif [10], [21] measured the complex refractive index of dust to model scattering and absorption behaviors. Alozie et al. [11] and Al-Bashir et al. [18] examined the impact of electromagnetic wave interactions with dust in the context of solar and wireless applications.

C. LiDAR and Visibility-Based Approaches

Visibility and LiDAR-based techniques have also been employed to estimate dust concentration and its optical effects. Shimizu et al. [12] used LiDAR-derived extinction coefficients to correlate with dust mass concentrations, validating visibility as a proxy for solar attenuation. The classical Koschmieder model [29] remains a foundational visibility-extinction relationship still used in atmospheric optics and remote sensing.

Despite these contributions, most models are either empirical or based on data from regions with different dust characteristics than Sudan. This study builds upon the existing literature by introducing a Sudan-specific, physics-based model that combines atmospheric optics, local dust particle data, and meteorological visibility records to predict PV system performance during dust storms more accurately.

3. METHODOLOGY

This study develops a semi-analytical model to estimate the normalized polarizability of dusty media composed of spherical particles, using electromagnetic theory and optical parameters at visible wavelengths (particularly at 500 nm). The methodology integrates theoretical modeling, simplification assumptions, and validation against standard results.

The modeling approach follows these sequential steps:

1. Physical Assumptions: Dust particles are modeled as homogeneous, isotropic spheres. The medium is optically thin, enabling use of single scattering theory. A monochromatic incident field at 500 nm is assumed. The surrounding medium is non-absorbing (e.g., air, with $\varepsilon_m \approx 1$).
2. Dielectric Properties and Polarizability: The complex dielectric function $\varepsilon_p=(n+j\kappa)^2$ is computed from known refractive indices of common dust types . Using the Clausius–Mossotti relation, the normalized polarizability per unit volume is derived in closed form for spherical particles. Experimental measurements found that n = 1.53 and n′ (k) = 0.008 at 500 nm. The single scattering albedo of Sudanese dust is approximately 0.96–0.98 across the visible spectrum.
3. Generalization: A general expression for ellipsoidal particles involving depolarization factors and elliptic integrals is presented, but detailed evaluation is deferred due to analytical complexity.
4. Macroscopic Modeling: For a medium with particle number density N, the effective susceptibility and optical depth τ are modeled using Beer–Lambert law. Real and imaginary parts of the polarizability are used to estimate scattering and absorption characteristics.
5. Numerical Evaluation: Parameters are evaluated numerically using refractive index data at 500 nm. Sensitivity analysis is conducted on particle radius, refractive index, and number density.
6. Meteorological Data Integration: Visibility data from four cities in Sudan—Khartoum, Abu Hamad, El Obeid, and Atbara—were used to model annual irradiance loss hours. This data was collected and averaged over five years by the Sudan Meteorological Department (SMD).

This methodology provides a basis for estimating the optical response of dusty media and forms the foundation for the mathematical models and simulation results discussed in the following sections.

4. PV PANELS PERFORMANCE

The annual energy output of a solar PV panel system depends on its efficiency, which is affected by factors such as latitude and climate. For a solar panel with an efficiency of η and an area of A m², under Standard Test Conditions (receiving a solar irradiance of 1000 W/m² for 2.74 hours per day), the energy generated over the course of the year, E, is expressed as:

$$E = 1000\, A\, \eta \quad \text{KWh} \qquad (1)$$

The PV panel can operate over a wide range of voltages and currents. The maximum power point of the panel is influenced by the intensity of incident sunlight. During dust storms, the solar irradiance at the panel surface decreases, which lowers the maximum power point. On the other hand, an increase in solar radiation can raise the panel's temperature, leading to a reduction in current production, which subsequently decreases the power output and impacts the overall efficiency [13].

The relationship between irradiance and the module's current and power can be expressed as follows:

$$\frac{G_1}{G_2}=\frac{I_2}{I_1}=\frac{P_2}{P_1} \quad (2)$$

Thus the reduction in panel output power is given by

$$P_{drop}=10\log\left(\frac{P_2}{P_1}\right)=10\log\left(\frac{I_2}{I_1}\right)=10\log\left(\frac{G_2}{G_1}\right) \text{ dB} \quad (3)$$

Where G_1 and G_2 are the irradiance values (in W/m²), I_1 and I_2 are the corresponding currents of the modules (in A), and P_1 and P_2 are the resultant powers when the irradiance changes (in W).

Studies in [14], [15], and [16] indicate that the output power of a PV panel increases with higher solar radiation. However, the power starts to decline once the solar radiation surpasses 800 W/m², even though the standard specifies that maximum power is attained at 1000 W/m². A key factor contributing to this behavior is the temperature of the panel, which often exceeds the standard temperature of 25°C. Figure 1 shows the correlation between solar irradiance attenuation (in dB) and the resulting decrease in output power based on these findings. This relationship can be expressed by the following power equation:

$$drop_{power}=0.613\left(att_{irrad}\right)^{(1.283)} \text{ dB} \quad (4)$$

where $drop_{power}$ represents the decrease in the panel's output power, measured in dB, and att_{irrad} denotes the attenuation in solar irradiance, also measured in dB.

Figure 1 illustrates a comparison between the measured and modeled drop in output power (dB) as a function of solar irradiance attenuation (dB). The close alignment between the two curves demonstrates the model's high accuracy in capturing the relationship between irradiance attenuation and power loss, indicating its reliability for assessing system performance under varying solar conditions.

5. MODEL DEVELOPMENT

This section develops a mathematical model to estimate the attenuation of solar irradiance due to dust particles suspended in air. We focus exclusively on spherical particles and express all relevant parameters in terms of the total number of particles N_T. This simplification allows for more direct application to real-world measurements and facilitates estimation from particle count data.

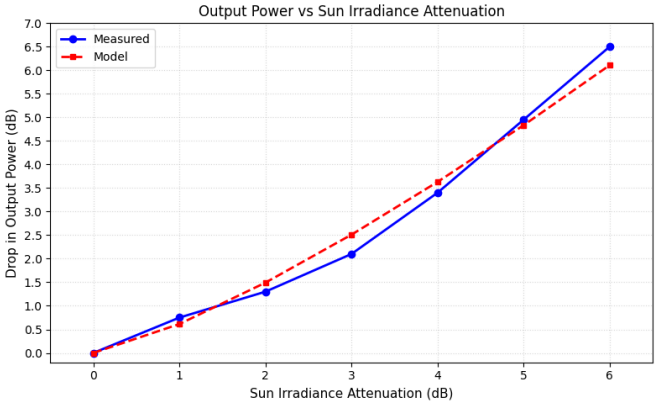

Figure 1: Relationship between solar irradiance attenuation and the drop in PV panel output power. The solid blue line with markers represents the measured values, while the red dashed line shows the model fitting.

A. Physical Assumptions

To derive a tractable model, the following assumptions are considered:

1. Geometry of the Dust Layer: The dusty medium is idealized as a slab of uniform thickness S and cross-sectional area A. The total volume of the slab is $V=A \cdot S$.
2. Particles: All dust particles are assumed to be homogeneous and perfectly spherical with radius r, and uniformly distributed within the medium [17], [18].
3. Dielectric Properties: Each particle has complex relative permittivity $\varepsilon_d=m^2=(n+jk)^2$, where n is the refractive index and k is the extinction coefficient [19]. The medium (air) is considered non-dispersive with $\varepsilon_m \approx 1$.
4. Radiative Effects:Particle interaction with incident light is dominated by absorption and elastic scattering, modeled using the extinction coefficient κ [20], [21].

B. Polarizability of a Particle

The interaction of an electromagnetic wave with a small particle can be modeled by treating the particle as an electric dipole. When exposed to an incident electric field $\vec{E}$, the induced dipole moment $\vec{p}$ is given by:

$$\vec{p}=\varepsilon_0 \varepsilon_m \alpha \vec{E} \quad (5)$$

where α is the (generally tensorial) polarizability of the particle, and ε_m is the permittivity of the surrounding medium.

For a general homogeneous ellipsoidal particle, the polarizability along the principal axis $i \in \{x,y,z\}$ is given by [18], [19]:

$$\alpha_i=V \cdot \frac{\varepsilon_d-\varepsilon_m}{\varepsilon_m+L_i\left(\varepsilon_d-\varepsilon_m\right)} \quad (6)$$

where:

- $V=\frac{4}{3}\pi abc$ is the volume of the ellipsoid,
- ε_d is the complex permittivity of the particle (dust in the present case),
- ε_m is the permittivity of the surrounding medium (air in the present case),
- L_i is the depolarization factor along axis i, satisfying $L_x+L_y+L_z=1$.

The values of L_i depend on the ellipsoid geometry and generally require elliptic integrals for evaluation. Closed-form expressions exist only for special symmetric cases (e.g., prolate or oblate spheroids), and even these can be algebraically complex [22]. For randomly oriented ellipsoids, orientation averaging further complicates the analysis. Consequently, analytical treatment becomes difficult, and such models are often approached numerically.

To simplify the analysis, it is assumed that the particles are perfect spheres with radius r, for which $L_i=1/3$ in all directions. The polarizability simplifies to :

$$\alpha=\frac{4}{3}\pi r^3\cdot\frac{\varepsilon_d-\varepsilon_m}{\varepsilon_d+2\varepsilon_m} \quad (7)$$

If the surrounding medium is air ($\varepsilon_m\approx1$):

$$\alpha=\frac{4}{3}\pi r^3\cdot\frac{\varepsilon_d-1}{\varepsilon_d+2} \quad (8)$$

This Clausius–Mossotti expression is widely used to describe the polarizability of small spherical particles in the Rayleigh scattering regime [17].

6. DUST REFRACTIVE INDEX AT VISIBLE LIGHT BAND

Studying the absorption and scattering processes requires an understanding of the complex refractive index of dust particles, which is determined by their chemical composition. The real part of the index, n, governs scattering, while the imaginary part, n', controls absorption [18].

The complex refractive index of mineral dust in the visible range (wavelengths approximately 400–700 nm) varies depending on composition, source region, and PSD, but typical values for Saharan or Sudanese dust are shown in Table 1.

Table 1: Dust refractive index at visible band

Wavelength (nm)	Real Part n	Imaginary Part k	Reference
440	1.53 – 1.59	0.003 – 0.006	[23], [24]
550	1.53 – 1.57	0.001 – 0.005	[23], [25]
670	1.50 – 1.55	0.0005 – 0.003	[24], [26]

The real part n indicates the phase speed of light through the medium. While the imaginary part k indicates the absorptive behavior of the dust (higher k means more absorption). For non-absorbing or weakly absorbing dust, k is very small (~0.001 to 0.005).

These values correspond to dust dominated by quartz, clay, feldspar, and iron oxides, typical in North African and Sudanese regions. Mineral dust from Sudan is often classified with the same optical properties as Saharan dust in remote sensing datasets such as AERONET and MODIS. For non-magnetic materials (a good approximation for most dust particles and atmospheric media), the relative permittivity ε_r is related to the refractive index n as:

$$\varepsilon_r=n^2 \quad (9)$$

where:

- ε_r is the relative permittivity (dielectric constant),
- n is the refractive index (real part if there is no absorption).

In the complex case, where the material absorbs radiation, both dielectric constant and refractive index become complex numbers:

$$\varepsilon=\varepsilon'+j\varepsilon''=(n'+jk)^2=n'^2-k^2+j2n'k \quad (10)$$

So:

- $\varepsilon'=n'^2-k^2$ real part of the dielectric constant (affects polarization),
- $\varepsilon''=2n'k$ imaginary part (related to absorption of electromagnetic waves).

A higher real part of the dielectric constant means the particle is more polarizable, affecting scattering and phase shift of radiation. While a higher imaginary part means the particle absorbs more light (linked to radiative attenuation). These values vary with wavelength, mineral composition, and particle structure [23].

A representative average value of the complex refractive index of desert mineral dust (including Sudanese or Saharan dust) in the visible range (around 550 nm) is commonly taken as: m=n+jk=1.53+i 0.003**.** This value is widely used in atmospheric radiative transfer models and aerosol studies as a standard optical constant for desert dust [23], [24]. It corresponds to moderately absorbing dust, with materials like clays, quartz, feldspar, and small amounts of iron oxides, typical in Sudan and North Africa and also balances empirical measurements from AERONET retrievals and laboratory spectroscopy.

For spherical particles, the polarizability α can be expressed using the classical Clausius-Mossotti relation derived from the particle's complex refractive index m=n+jk and radius r. At wavelength λ=500 nm assuming the particle is small compared to the wavelength (Rayleigh regime), the polarizability. α is given by Equation (6) can be rewritten in terms of refractive index as:

$$\alpha=4\pi r^3\varepsilon_0\frac{m^2-1}{m^2+2} \quad (11)$$

where:

- r is the particle radius (in meters),
- ϵ_0 is the vacuum permittivity $\approx8.854\times10^{-12}$ F/m,
- m=n+jk is the complex refractive index at λ=500 nm.

Typical complex refractive index for mineral dust particles at 500 nm is approximately m=1.53+i 0.005 [28]. Thus, at 500 nm we have

$$\mathcal{R}(\alpha)=1.39\times10^{-29}\times0.3086\approx4.29\times10^{-30}\,\mathrm{Fm}^2$$
$$\mathcal{I}(\alpha)=1.39\times10^{-29}\times0.00243\approx3.38\times10^{-32}\,\mathrm{Fm}^2 \quad (12)$$

7. DUST PARTICLE SIZE DISTRIBUTION

Dust consists of a heterogeneous mixture of various mineral components, including quartz, corundum, hematite, calcium carbonate, magnesium carbonate, calcium sulfate, and manganese oxide. Among these, quartz is the most abundant, comprising approximately 60% of the dust composition [36]. During dust storms, strong winds mobilize large quantities of sand and dust from dry, exposed soil surfaces, lifting the particles into the atmosphere and enabling their transport over long distances.

Although all scattering models require the assumption of a consistent particle shape, naturally occurring dust particles exhibit highly irregular and varied geometries. These range from needle-like structures to nearly spherical or disc-like shapes, making precise modeling of their optical behavior a complex task. To simplify analysis, researchers often approximate dust particles as spheres, particularly when studying their influence on light transmission. The equivalent diamete**r** of a spherical particle refers to the diameter of a sphere that behaves similarly to the irregular dust particle when suspended in a fluid. However, this simplification can introduce significant errors in scattering and radiative transfer calculations, especially when the actual particle shapes deviate considerably from spheres.

Dust samples collected from central and northern Sudan revealed that the airborne particles typically have equivalent diameters ranging from 11 μm (μm) to 75.3 μm (μm), with these values representing the minimum and maximum observed sizes, respectively [37]. The probability density function (PDF) describing the size distribution of these particles, often referred to as the number distribution function, is defined in Appendix A as a function of the particle diameter D

$$n(D)=\frac{2.48\times10^{-10}}{D^3} \quad (13)$$

where D is the particle diameter in meters.

Visible light wavelengths range approximately from 400 nm to 700 nm, which are considerably shorter than typical dust PSD. A key parameter in understanding light interaction with dust is the size parameter ϑ, defined as the ratio of the particle's circumference to the wavelength of the incident light [38].

$$\vartheta=\frac{2\pi r}{\lambda} \quad (14)$$

For visible wavelengths, particularly around 500 nm, the size parameter ϑ for dust particles typically ranges from 11 to 73.5 in average, indicating that these particles are significantly larger than the wavelength of the probing light [39]. Given this large size ratio ($\vartheta \gg 10$), the scattering behavior of dust particles is governed primarily by geometric optics phenomena such as reflection, refraction, diffraction, and transmission at the particle-air interface and within the particle itself [40]. Consequently, classical scattering theories such as Rayleigh or Mie scattering are inadequate for modeling light interaction with dust in the visible spectrum. Instead, geometric optics provides a more suitable framework for describing absorption and scattering by such large particles [41].

8. LIGHT SCATTERING BY DUST PARTICLE

Airborne dust particles can scatter and absorb electromagnetic radiation (solar radiation) at different wavelengths [17]. Scattering is a process, which conserves the total amount of energy, but the direction in which the radiation propagates may be altered. On the other hand, absorption is a process that removes energy from the electromagnetic radiation field, and converts it to another form. Extinction (or attenuation) is the sum of scattering and absorption effects, so it represents total effect of medium on radiation propagates it.

The cross-sections for scattering, absorption, and extinction (σ), along with the efficiency (Q) and coefficient (κ) for a single dust particle, are related by the following equation.

$$\kappa_{sc}=N_T\sigma_{sc}=N_T\left(\frac{\pi D^2}{4}\right)Q_{sc} \quad (15a)$$

$$\kappa_{\mathrm{abs}}=N_T\sigma_{\mathrm{abs}}=N_T\left(\frac{\pi D^2}{4}\right)Q_{\mathrm{abs}} \quad (15b)$$

$$\kappa_{ext}=N_T\sigma_{ext}=N_T\left(\frac{\pi D^2}{4}\right)Q_{ext} \quad (15c)$$

N_T represents the number concentration of particles with a diameter of D. The Q terms (unitless) are referred to as the single particle extinction, scattering, or absorption efficiency parameter, depending on the effect being described. $\zeta_{ext} = \zeta_{sc} + \zeta_{abs}$ and their units are inverse length.

The complexity of the scattering problem increases when considering the particle's geometry relative to the incident light beam. In this study, however, we simplify the analysis by assuming spherical particle shapes, as discussed in prior works [42]. The single-particle scattering efficiency Q_{scat} for these spherical particles can be expressed as the sum of three components, each corresponding to a distinct optical effect:

$$Q_{scat}=Q_{diff}+Q_{reft}+Q_{tr} \quad (16)$$

Where Q_{diff}, Q_{ref}, and Q_{tr} represent the efficiencies of diffraction, reflection, and transmission, respectively. For dust particles, the diffraction efficiency Q_{diff} is generally assumed to be unity [43]. The extinction coefficient κ quantifies the total loss of light intensity per unit path length in the atmosphere. In dusty air, this loss results from two primary mechanisms:

$$\kappa=\kappa_{\mathrm{scattering}}+\kappa_{\mathrm{absorption}} \quad (17)$$

Where:

- $\kappa_{\mathrm{scattering}}$ accounts for light scattered by suspended dust particles,
- $\kappa_{\mathrm{absorption}}$ includes absorption by both dust particles and air molecules.

In clean atmospheric conditions, the extinction coefficient is relatively small, typically ranging between 10^{-5} and 10^{-4} m^{-1} [44]. However, in dust-laden air, particularly during dust storms, it can increase significantly—ranging from 10^{-3} m^{-1} up

to values exceeding 1 m^{-1}, depending on the dust concentration, PSD, and the wavelength of incident light [45]. As shown in Section 7, dust particle size is comparable to or larger than the wavelength. Thus geometric optics regime is used here, instead of Mie scattering theory.

In the geometric optics regime, applicable when dust particle diameters are significantly larger than the wavelength of visible light ($D \gg \lambda$), the scattering of solar radiation by dust particles is dominated by diffraction and surface reflection. Table 1 shows the absorption, scattering and extinction efficiency for dust particles in the range from 10 to 80 micron, which correspond to large dust particle sizes, as mentioned in Section 7. These values are obtained by geometrical optics approximations.

Table 2:Dust Extinction Efficiency for Large Particles (λ = 550 nm)

Radius (μm)	r Size Parameter	Q_{abs}	Q_{sca}	Q_{ext}
10	114.2	~0.70	~1.80	~2.50
20	228.4	~0.65	~1.85	~2.50
30	342.6	~0.60	~1.90	~2.50
40	456.9	~0.55	~1.95	~2.50
50	571.2	~0.50	~2.00	~2.50
60	685.4	~0.45	~2.05	~2.50
70	799.7	~0.40	~2.10	~2.50
80	913.9	~0.35	~2.15	~2.50

In the 10–80 μm size range, extinction efficiency remains approximately constant at about 2.5. This value is mostly independent of composition or refractive index at such large D. Absorption efficiency decreases, while scattering dominates.

Changes in the dust PSD necessitate adjustments in the optical properties of the dusty medium. Under such conditions, the extinction coefficient can be calculated using the following expression, with $Q_{ext} = 2.5$:

$$\kappa_{ext} = \int_0^d \frac{2.5\pi D^2}{4} N(D)\, dD \tag{18}$$

The size distribution of dust particles is denoted by N(D), which represents the number of particles per unit volume with a given diameter D. Incorporating this distribution into the analysis, the expression for the total number of particles N_T can be reformulated as:

$$N_T = \int_{D_{min}}^{D_{max}} N(D).\, dD = N_T \int_{D_{min}}^{D_{max}} n(D)\, dD \tag{19}$$

This integral accounts for the entire range of particle-sizes present in the dust sample, from the minimum diameter D_{min} to the maximum diameter D_{max}, providing a more accurate representation of the particle population within the medium. n(D) is the number distribution function defined in Equation (14). Thus Equation (19) can be rewriting as:

$$\kappa_{ext} = \frac{2.5\pi N_T}{4} \int_{D_o}^{D_h} D^2 n(D)\, dD \tag{20}$$

Equation (19), (20) and (21) include N(D) dD which represents the number of dust particles with diameters between D and D+dD, n(D) indicating the distribution of dust particles by number, D_{min} and D_{max} as the largest and smallest diameters in the dust sample, and N_T as the overall count of soil particles in the air n(D) is normalized particle-size probability density function.

Substitute for n(D) and carrying the integration with limit from $D_o = 11 \times 10^{-6}$ m and $D_h = 73.5 \times 10^{-6}$ m (see Appendix A), the dusty air extinction coefficient is given by:

$$\kappa_{ext} = 9.248 \times 10^{10} N_T \quad m^{-1} \tag{21}$$

The single scatter albedo (ω) is an important parameter that can also characterize the optical properties of the medium. Single scattering albedo is a key aerosol optical characteristic in assessment the radiative effects due to aerosols. It is defined as the ratio of the scattering and extinction cross sections or the corresponding Q terms.

$$\omega = \frac{\sigma_{scat}}{\sigma_{ext}} = \frac{Q_{scat}}{Q_{ext}} \tag{22}$$

Values of 0.96 and 0.98 have been reported in the literature for the albedo of dust particles at wavelengths of 537 nm and 637 nm, respectively.

9. EXTINCTION COEFFICIENT AND VISIBILITY MODEL

Visibility refers to the maximum distance at which distinct objects can be seen with the naked eye under atmospheric conditions. It is a key atmospheric parameter commonly reported in meteorological observations. Visibility can be significantly reduced by airborne particles such as smoke, pollutants, moisture, fog, and dust. Among these, dust is particularly relevant in arid regions and has been widely studied due to the availability of long-term visibility records from numerous observation stations within the World Meteorological Organization (WMO) network.

Although the concentration of dust particles in the air provides a more direct and accurate measure of mineral dust content, horizontal visibility remains a useful indicator for estimating the attenuation of solar radiation caused by suspended dust. In meteorology, the severity of a dust storm is often assessed through visibility metrics, which decline as the intensity of airborne dust increases.

Fractional dust relative volume for particles with diameters in the range D to D + δD

$$\delta v = \frac{\pi D^3}{3} N(D)\, \delta D \tag{23}$$

Since the size of dust particles varies greatly [4], the relative volume v of dust is given by:

$$v = \frac{a'\pi N_T}{6} \int_{D_o}^{D_h} dD = 8.116 \times 10^5 \times N_T \tag{24}$$

The dust relative volume is related to visibility during a dust storm (V, km) by [12]:

$$v = \frac{9.43 \times 10^{-9}}{V^{1.07}} \quad (25)$$

Here visibility is measured in km. Therefore, the total number of dust particles per unit volume of air is related to visibility.

$$N_T = \frac{1.162 \times 10^{-14}}{V^{1.07}} \quad (26)$$

Substituting value in Equation (22). extinction coefficient of dusty medium (air with suspended dust particles) is given by

$$\kappa_{ext} = \frac{1.075}{V^{1.07}} \quad (27)$$

Koschmieder model relates the extinction coefficient to visibility by the relationship

$$\zeta_{ext} = \frac{K}{V} \quad (28)$$

This model is widely used in atmospheric optics and meteorology to quantify visibility reduction due to scattering and absorption by airborne particles such as dust, fog, or smoke.

The Koschmieder constant K is derived based on the minimum contrast sensitivity of the human eye, which typically ranges from 2% to 5%. It represents the contrast threshold at which an object just becomes visible against the sky at the horizon. According to Middleton (1952) [29], assuming a contrast threshold of 2%, and expressing the horizontal extinction coefficient ζ_{ext} in Mm^{-1} (inverse megameters), K=3.192.

To evaluate the performance of the present empirical extinction model, a comparison was made with the classical Koschmieder model, which is based on a contrast threshold of 2%, Figure 2. Structurally, the Koschmieder model assumes a linear inverse relationship between visibility and extinction coefficient, whereas the present model introduces a slightly steeper power-law dependence with an exponent of 1.07. At low visibility ranges (less than 1 km), the Koschmieder model consistently predicts significantly higher extinction values, reflecting its conservative nature and suitability for safety-critical applications such as aviation and transportation. In contrast, the present model yields lower extinction coefficients, suggesting it is more representative of real-world observations in hazy, dusty, or polluted conditions. While the Koschmieder model provides a theoretical upper bound on extinction, the empirical model offers improved accuracy for atmospheric conditions deviating from ideal assumptions, making it valuable for practical modeling purposes where precision rather than conservatism is required.

10. SOLAR IRRADIANCE AND DUST STORMS

Saharan dust affects the amount of solar irradiance reaching the Earth's surface as mentioned previously. Previous studies [24], [25] , [26], [27] have shown the impact of dust storms on light propagation through a dusty medium can be analyzed by examining the optical depth of the medium. The optical depth indicates the level of attenuation due to absorption and scattering that occurs as light passes through the dust storm. Higher optical depths in dusty medium can significantly reduce surface radiation, potentially posing a threat to photovoltaic systems.

$$\zeta_{ext} = \frac{K}{V} \quad (29)$$

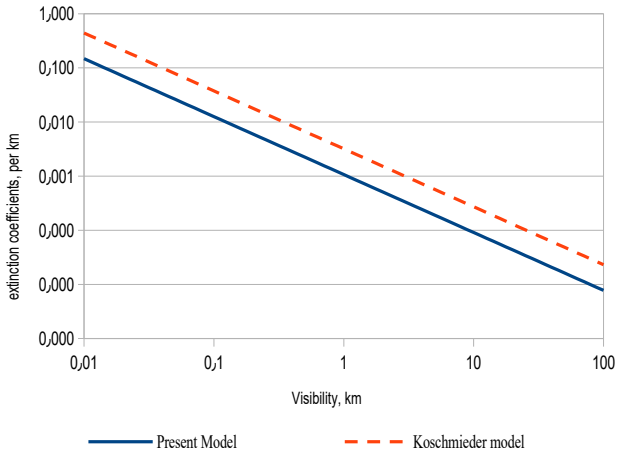

Figure 2: Extinction coefficient of a dusty medium as a function of visibility. The solid blue line represents the present model, while the red dashed line corresponds to the Koschmieder model.

For a homogeneous dust layer with uniform properties, the optical depth simplifies to:

$$\zeta_{ext} = \frac{K}{V} \quad (30)$$

$$\tau(\lambda) = \kappa(\lambda) \cdot h \quad (31)$$

where:

- $\tau(\lambda)$ is the optical depth (dimensionless),
- $\kappa(\lambda)$ is the extinction coefficient [m^{-1}],
- h is the thickness of the dust layer [m].

There are numerous computational and analytical methods available for solving the radiation transfer equation, which takes into account multiple scattering, absorption, and emission by atmospheric dust particles and gases. When considering single scattering, one can use the Beer-Lambert law to determine the intensity of light, ς, at a given distance z, taking into account the attenuation caused by atmospheric aerosols with extinction coefficient κ_{ext}.

$$\frac{I}{I_0} = e^{-\zeta_{ext} z} = e^{-\tau} \quad (32)$$

The medium optical depth, represented by τ ($=\kappa_{ext}$ z), and the incident intensity, represented by I_0, are both important factors to consider. The consideration of dust particles changes with height, therefore the extinction coefficient should also be dependent on both height and optical depth.

11. VISIBILITY STATISTICS DURING DUST STORMS

As mentioned in Section 9, the visibility refers to the maximum distance in the atmosphere towards the horizon where distinct objects can be seen without the use of any aids, (with the naked eye). It is a significant atmospheric factor often included in meteorological reports. Various airborne particles like smoke, pollution, moisture, fog, and dust can reduce visibility. Visibility is frequently studied in relation to dust, as it is readily available from multiple observation stations within the World Meteorological Organization (WMO) network for long periods of time. However, the concentration of dust in the air is a more precise measure of mineral dust levels compared to visibility. Nevertheless, horizontal visibility can be used to estimate the reduction in solar radiation caused by suspended dust particles.

Using data collected by the Sudan Meteorological Department on visibility measurements in different towns in Sudan is advantageous. Table 3 provides statistics on visibility recorded in four towns, showing the average observations over a five-year time frame. The total hours listed represent the duration of visibility within a specified range.

Table 3: Visibility Statistics in Sudan

Visibility (meter)	Visibility (Hrs/Annual)			
	Khartoum	Abu Hamad	El Obied	Atbara
000-100	3.80	0.61	2.37	0.79
100-200	5.40	4.82	4.03	1.59
200-300	6.13	4.03	6.22	1.60
300-400	7.27	7.53	3.77	6.18
400-500	6.75	2.45	4.20	3.85
500-600	8.41	15.16	4.56	6.75
600-700	3.77	19.62	2.63	8.76
700-800	2.63	6.83	0.35	10.16
800-900	21.64	17.34	13.67	17.43
900-1000	0.79	9.11	1.40	4.38

Figure 3 displays the yearly hours with visibility below V. This correlation is best depicted by power equations.

$$T(V)=1.70\times10^{-3}V^{1.53} \tag{33}$$

T(V) is the time it takes for an annual visibility to decrease by V.

The annual hours with visibility below V is the best fit with Equation (33).

$$\kappa_{ext}=\frac{2.27}{V^{1.07}} \quad km^{-1} \tag{34}$$

It is noticed that the constant in Equation (33) is greater than the constant derived for viability model in Section 9, but lower than Koschmieder constant. This variation is believed to be due to the nature and properties of dust and model assumptions.

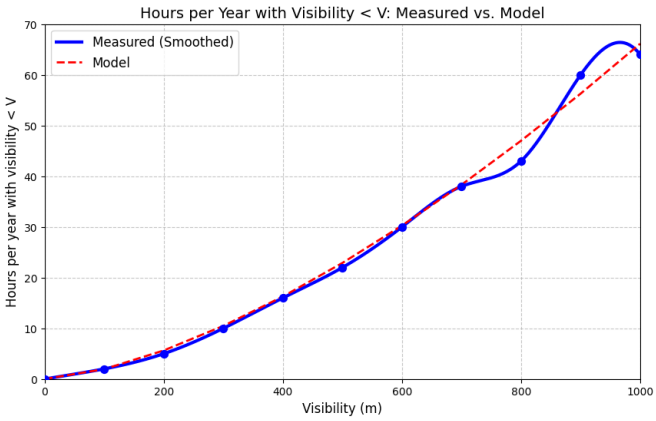

Figure 3: Annual hours with visibility less than V. The solid blue line with markers represents the smoothed measured data, while the red dashed line shows the model results.

12. MODEL FOR PV SYSTEM PERFORMANCE DURING DUST STORMS

During a dust storm, extinction coefficients often vary with altitude, reflecting changes in both PSD and visibility at different heights. The effective signal path length through the dust layer, denoted as L, depends on the sun's elevation angle θ, Figure 5. This path length can be estimated using the following relationship:

$$L=\frac{h}{\sin(\theta)} \tag{35}$$

Where:

- L is the signal path through the dust storm,
- h is the vertical thickness of the dust layer,
- θ is the sun's elevation angle.

This geometric relationship highlights how lower sun angles (e.g., during sunrise or sunset) result in a longer path through the dusty atmosphere, thereby increasing extinction effects.

The visibility at any height h within the storms is related to visibility (V_o) at a specific height (h_o), reference measurement height, by [33].

$$V(h)-V_o\left[\frac{h}{h_o}\right]^{0.26} \tag{36}$$

Visibility at a given height h is calculated based on a reference visibility V_0 measured at a specific reference height h_0. According to Equation (36), visibility varies along the propagation path of solar radiation and is not uniform with altitude. Since the Sudan Meteorological Department records visibility at a standard height of 15 meters above ground level, Equation (36) is applied using this reference data to evaluate how visibility changes with height.

$$V(h)=2.98\,V_O h^{0.26} \tag{37}$$

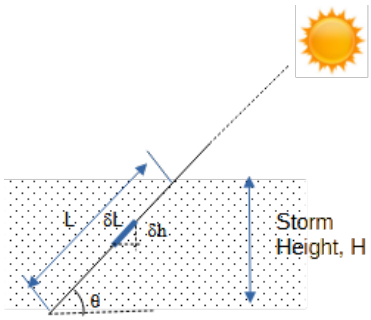

Figure 5: Effective path of a light beam passing through a dust storm. The diagram illustrates the storm height H, the light path length L, the incremental path δL, and the corresponding height difference δh at an incidence angle θ.

Therefore, the dusty medium has an optical depth of $\kappa_{ext}\delta L$ (=δτ).over any given path δL, as illustrated in Figure 5. Using classical Koschmieder model, since it represents the worst case , we get

$$\delta\tau=\kappa_{ext}\delta L=\frac{3.912}{V}\frac{\delta h}{\sin\theta}$$
$$=\frac{3.912}{2.98\,h^{0.26}V_O}\frac{\delta h}{\sin\theta}=\frac{1.313}{h^{0.26}V_O}\frac{\delta h}{\sin\theta} \tag{38}$$

The total optical depth over the storm height H is

$$\tau=\frac{1.313}{V_o\sin(\theta)}\int_0^H\frac{1}{h^{0.26}}dh$$
$$=\frac{1.313}{V_o\sin(\theta)}\times\frac{H^{0.74}}{0.74}=\frac{1.774\,H^{0.74}}{V_o\sin(\theta)} \tag{39}$$

For storms with 3 km height (typical height)

$$\tau=\frac{3.991}{V_o\sin(\theta)} \tag{38}$$

The attenuation in solar radiation intensity is

$$att=e^{\tau} \tag{39}$$

13. PV SYSTEM PERFORMANCE EVALUATION

The developed model is applied to quantify the reduction in solar irradiance and corresponding PV output during dust storms in Sudan, taking into account variations in visibility and sun elevation angle.

13.1. Irradiance Attenuation During Dust Storms

As established in Section 12, the total optical depth (τ) for a dust storm of height H and visibility V_o at reference height h_o is given Equation (38) and optical attenuation is given by Equation (39). Figure 6 illustrates the relationship between optical depth and visibility during a dust storm. The graph shows how the optical depth increases as visibility decreases, which is a common observation during dust storms. Optical depth is a measure of the extent to which particles in the atmosphere, such as dust, reduce the transmission of light. As dust particles accumulate in the atmosphere, they scatter and absorb sunlight, causing the optical depth to increase. The decrease in visibility reflects the reduced amount of light reaching the observer due to the scattering and absorption caused by dust particles. In the figure, as the optical depth rises, visibility is observed to drop significantly, indicating that higher levels of dust concentration in the atmosphere result in poorer visibility. This is particularly important for understanding the impact of dust storms on both environmental visibility and solar energy transmission. Generally, these results show that as visibility decreases and sun elevation angle drops, the path length through the dusty medium increases, resulting in greater irradiance losses.

13.2. Attenuation vs. Sun Angle and Visibility

Figure 7 illustrates the predicted attenuation (in dB) for a 3 km dust storm across a range of sun elevation angles and visibility levels. The results confirm that:

- Lower sun angles (e.g., morning or evening) lead to significantly higher attenuation due to increased optical path length through dust.
- Visibility below 500 m can cause irradiance losses exceeding 10 dB, corresponding to PV output losses of 50% or more.

This figure demonstrates that solar irradiance attenuation is not only a function of the amount of dust in the atmosphere (as indicated by visibility) but also depends on the sun's elevation angle. These insights are vital for understanding how dust storms impact both visibility and solar energy harvesting, as well as for developing models to predict the effects of atmospheric dust on solar irradiance.

The results emphasize the importance of considering diurnal variations and local meteorological visibility in solar forecasting and system planning.

13.3. Incorporating Real PV Data

To strengthen model validation, it is recommended to compare the theoretical predictions with real PV performance data from operational systems in Sudan or similar arid regions.

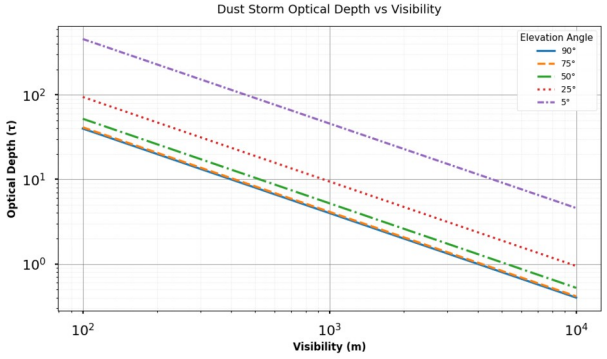

sar

Figure 6: Variation of optical depth (τ) with visibility during a dust storm at different elevation angles. The curves represent elevation angles of 90°, 75°, 50°, 25°, and 5°.

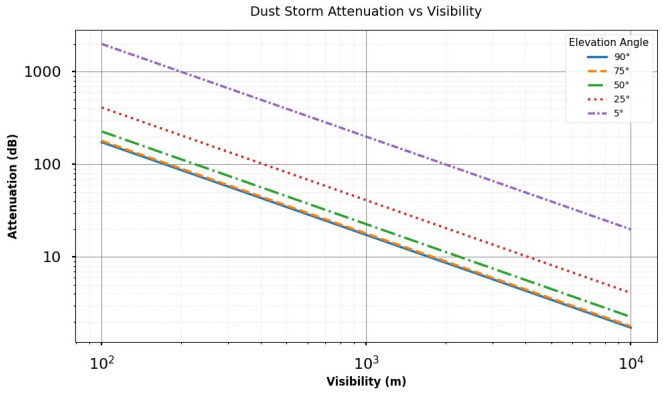

Figure 7: solar irradiance attenuation as a function of visibility for a dust storm height of 3 km at different solar elevation angles 90º, 75º, 50º, 25º, and 5º.

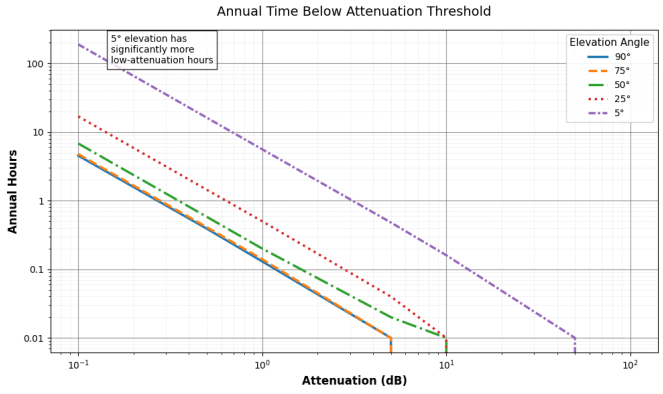

Figure 8: Annual hours during which the attenuation of solar irradiance due to dust storms in Sudan is less than a given threshold, for different solar elevation angles (90º, 75º, 50º, 25º, and 5º).

This could include:

- Hourly/daily output logs from PV systems during known dust storm periods,
- Satellite-based irradiance estimates (e.g., from NASA POWER, MERRA-2, or SARAH-2),
- On-site pyranometer or irradiance sensor data, where available.

Such comparisons would help:

- Quantify the model's accuracy in real-world conditions,
- Calibrate extinction coefficients more precisely,
- Account for secondary factors like soiling losses, ambient temperature, and diffuse irradiance gain during dust events

14.2. Geographic Generalizability

While the model is tailored for Sudanese dust characteristics, it is readily adaptable to other arid and semi-arid regions by adjusting the following inputs:

- Particle size distribution (PSD)
- Refractive index (n, k) specific to local dust composition
- Visibility statistics from regional meteorological stations
- Dust layer height and typical storm profiles

14. MODEL VALIDATION AND LIMITATIONS

This section assesses the validity and applicability of the proposed dust attenuation model by comparing it with real-world findings from similar climatic regions and discussing its limitations and broader relevance.

14.1. Predicted Output Losses vs. Published Data

Using Sudan-specific parameters—visibility data, particle size distributions, and refractive index values—the model predicts PV output reductions of:

- 30–50% during severe dust events (visibility < 300 m)
- 10–20% under moderate conditions (visibility 500–800 m)

These results align closely with studies from neighboring countries in the MENA region:

Study / Source	Region	Reported Output Reduction	Environmental Conditions	Notes
Pourasl et al. (2023) [3]	Global/ MENA	20–40%	High dust deposition	Literature review
Chaichan et al. (2023) [9]	Baghdad, Iraq	28–52%	Monthly exposure without cleaning	Similar dust density and storm pattern
Kosmopoulos et al. (2017) [8]	MENA	15–35%	Measured AOD and irradiance loss	Radiative transfer modeling
Bamisile et al. (2025) [4]	UAE & Egypt	25–45%	Multi-week dust storm periods	Field measurements

Regions such as the Sahel, Sahara, Arabian Peninsula, and parts of South Asia exhibit similar dust behavior, making the model suitable for application across the MENA and Global South. However, in humid environments or locations with significant non-mineral aerosols (e.g., biomass smoke, industrial pollution), the model may overestimate irradiance loss unless absorption coefficients are recalibrated accordingly.

14.3. Strengths

The proposed model exhibits several notable strengths that enhance its applicability and reliability in analyzing dust storm effects on solar irradiance.

1. Integrates physical optics, meteorological visibility, and particle-level physics.
2. Provides predictive capability, not just empirical correlation.

3. Applicable with minimal site data (visibility and dust size range).

14.4. Limitations and Future Work

While initial validation is promising, the model has several limitations that should be acknowledged, which in turn highlight opportunities for future work and refinement:

1. Lack of field-level PV performance data from Sudan to enable direct comparison and calibration.
2. Simplifying assumptions include:
   - Spherical particle geometry
   - Uniform vertical dust concentration
3. Neglect of soiling effects, which may exacerbate PV losses in long-duration storms.
4. Neglect of diffuse irradiance increase during scattering-dominated conditions.

14.4. Recommended Further Work:

To strengthen the applicability and reliability of the proposed model, the following areas are recommended for further research and development:

1. Collaborate with local photovoltaic (PV) system operators to gather real-world energy output data during dust storm events.
2. Incorporate satellite-derived Aerosol Optical Depth (AOD) data, such as from MODIS or AERONET, to enable wider spatial validation.
3. Enhance the model by accounting for non-spherical dust particle effects and incorporating diurnal variations in solar irradiance.

15. CONCLUSION

This paper introduced a semi-analytical model for predicting the degradation of photovoltaic (PV) system performance under dusty atmospheric conditions, using Sudan as a case study. The model incorporates physical particle-level parameters, electromagnetic theory, and meteorological visibility data to estimate irradiance attenuation and its impact on PV output. It addresses key limitations in existing empirical models by offering a physics-based approach tailored to local environmental conditions.

The results indicate that dust storms, particularly under low visibility and low solar elevation angles, can cause substantial energy losses—reaching up to 50% during severe events. These findings align with reported data from other arid regions, confirming the model's reliability and potential for broader application.

Future work will focus on enhancing the model through integration of satellite-based aerosol optical depth (AOD) data (e.g., from MODIS or AERONET) to improve spatial resolution. Additionally, coupling the model with machine learning techniques could enable AI-driven forecasting of PV performance under dynamic atmospheric conditions, providing a valuable tool for energy planners and grid operators in dust-prone environments.

AI Writing Disclosure

The author used ChatGPT (OpenAI) to assist with drafting and improving the clarity of this manuscript. All content was reviewed and edited, and the author assumes full responsibility for its accuracy and originality.

REFERENCES

[1]. IRENA, "Renewable Capacity Statistics 2023," International Renewable Energy Agency, 2023.

[2]. J. D. Farmer and F. Lafond, "How predictable is technological progress?", "Research Policy", vol. 45, pp. 647–665, 2016.

[3]. H. H. Pourasl, R. V. Barenji, and V. M. Khojastehnezhad, "Solar energy status in the world: A comprehensive review,", "Energy Reports", vol. 10, pp. 3474–3493, Nov. 2023.

[4]. O. Bamisile et al., "The environmental factors affecting solar photovoltaic output,", "Renewable and Sustainable Energy Reviews", vol. 208, p. 115073, 2025.

[5]. P. Sarmah et al., "Comprehensive analysis of solar panel performance and correlations with meteorological parameters,", "ACS Omega", vol. 8, no. 50, pp. 47897–47904, Dec. 2023.

[6]. L. Liu et al., "Prediction of short-term PV power output and uncertainty analysis,", "Applied Energy", vol. 228, pp. 700–711, 2018.

[7]. A. Papachristopoulou et al., "15-Year analysis of direct effects of total and dust aerosols in solar radiation/energy over the Mediterranean Basin,", "Remote Sens.", vol. 14, no. 7, p. 1535, 2022.

[8]. D. Kosmopoulos et al., "Dust impact on surface solar irradiance assessed with model simulations, satellite observations and ground-based measurement,", "Atmos. Meas. Tech.", vol. 10, pp. 2435–2453, 2017.

[9]. M. T. Chaichan et al., "Sand and dust storms' impact on the efficiency of the photovoltaic modules installed in Baghdad: A review study with an empirical investigation,", "Energies", vol. 16, no. 9, 2023.

[10]. M. Masoom et al., "Forecasting dust impact on solar energy using remote sensing and modeling techniques,", "Solar Energy", vol. 228, pp. 317–332, 2020.

[11]. A. Monteiro et al., "Multi-sectoral impact assessment of an extreme African dust episode in the Eastern Mediterranean in March 2018,", "Science of the Total Environment", vol. 843, 2022.

[12]. S. Ghobrial and S. Sharif, "Microwave attenuation and cross polarization in dust storms,", "IEEE Trans. Antennas Propag.", vol. 35, no. 4, pp. 418–425, Apr. 1987.

[13]. S. Odeh, "Analysis of the performance indicators of the PV power system,", "J. Power Energy Eng.", vol. 6, pp. 59–75, 2018.

[14]. E. Alozie et al., "A review of dust-induced electromagnetic waves scattering theories and models for 5G and beyond wireless communication systems,", "Scientific African", vol. 21, 2023.

[15]. J. E. Lindberg et al., "Measurement of the absorption coefficient of atmospheric dust,", "Appl. Opt.", vol. 13, no. 8, pp. 1923–1927, 1974.

[16]. I. F. Eldehn, M. M. El-Halwagi, and M. S. El-Sayed, "Influence of solar radiation and module temperature on

solar module performance,", "MJAEE Journal", vol. 13, no. 2, pp. 36–40, 2020.
[17]. N. A. Nasrin, M. A. Alghoul, M. S. M. Ali, and H. A. Mohammed, "Effect of high irradiation on photovoltaic power and energy,", "Renewable Energy", vol. 116, pp. 552–569, 2018.
[18]. M. A. Al-Bashir, M. A. Hannan, and A. Mohamed, "Analysis of effects of solar irradiance, cell temperature and wind speed on photovoltaic systems performance,", "Int. J. Energy Econ. Policy", vol. 10, no. 1, pp. 354–360, 2020.
[19]. J. Haywood and O. Boucher, "Estimates of the direct and indirect radiative forcing due to tropospheric aerosols: A review,", "Rev. Geophys.", vol. 38, 2000.
[20]. R. Román and M. Antón, "Evaluation of the desert dust effects on global, direct and diffuse spectral ultraviolet irradiance,", "Tellus B: Chem. Phys. Meteorol.", vol. 65, no. 1, 2013.
[21]. S. M. Sharif, "Attenuation properties of dusty media using Mie scattering solution,", "Prog. Electromagn. Res. M", vol. 43, pp. 9–18, 2015.
[22]. S. M. Sharif, "Chemical and mineral composition of dust and its effect on the dielectric constant,", "IEEE Trans. Geosci. Remote Sens.", vol. 33, no. 2, pp. 353–359, Mar. 1995.
[23]. I. Tegen, "Modeling the mineral dust aerosol cycle in the climate system,", "Quat. Sci. Rev.", vol. 22, no. 18–19, pp. 1821–1834, 2003.
[24]. C. Pérez et al., "Interactive dust-radiation modeling: A step to improve weather forecast,", "J. Geophys. Res.", vol. 111, D16206, 2006.
[25]. Y. Balkanski et al., "Reevaluation of mineral aerosol radiative forcings suggests a better agreement with satellite and AERONET data,", "Atmos. Chem. Phys.", vol. 7, pp. 81–95, 2007.
[26]. B. Heinold et al., "Dust radiative feedback on Saharan boundary layer dynamics and dust mobilization,", "Geophys. Res. Lett.", vol. 35, L20817, 2008.
[27]. K. Schepanski, "Transport of mineral dust and its impact on climate,", "Geosciences", vol. 8, no. 151, 2018.
[28]. D. A. Gillett, "Environmental factors affecting dust emission by wind erosion," in "Saharan Dust", C. Morales, Ed. New York, NY, USA: Wiley, 1979.
[29]. W. E. K. Middleton, "Vision Through the Atmosphere". Toronto, Canada: Univ. Toronto Press, 1952.
[30]. A. Shimizu et al., "Relationship between LiDAR-derived dust extinction coefficients and mass concentrations in Japan,", "SOLA", vol. 7A, pp. 001–004, 2011.
[31]. S. M. Sharif, "Dust particles-size distribution," in "Proc. Int. Geosci. Remote Sens. Symp. (IGARSS'87)", Michigan, USA, May 1987.
[32]. H. Horvath, "On the applicability of the Koschmieder visibility formula,", "Atmos. Environ.", vol. 5, no. 3, pp. 177–184, Mar. 1971.
[33]. S. M. Sharif, "Performance of Earth-Satellite Links During Dust Storms at the X-Band ," "SES Journal ", vol. 40, no. 33, pp. 14–19, 1993.

APPENDIX A

Dust Particle-Size Distribution (PDS)

Several researchers have studied the particle-size distribution (PSD) of dust, but the reported distributions in literature vary greatly, making it challenging to identify a consistent pattern. In order to analyze the dust PSD, samples were collected from northern and central Sudan in 1981, 1982, and 1983. The PSD analysis was carried out using the hydrometer and pipette methods, which are founded on Stocks' law of sedimentation. The findings suggested that the cumulative curves of dust PSD can be reasonably represented by a linear equation [26].

$$f(D)=a+bD \tag{A1}$$

The weight fraction of particles with an equivalent diameter less than D μm, denoted as f(D), and constants a and b, which vary depending on factors such as source soil conditions, distance from the source, and meteorological factors, determine the fraction of mass formed by particles with diameters between D and D+δD.

$$\delta M=\left(a+b\left(D+\delta D\right)\right)-\left(a+b\left(D\right)\right)=b\,\delta D \tag{A2}$$

The fractional volume occupied by particles with diameters ranging from D to δD is.

$$\delta v=\frac{\delta M}{\rho} \tag{A3}$$

The density of dust, denoted as ρ, is equal to 2430 kgm-3. Therefore, the number of dust particles responsible for the fractional mass δM can be determined as follows.

$$\delta N=\frac{6\,b\,\delta D}{\rho\,\pi\,D^3} \tag{A4}$$

The number of dust particles δN within the range of diameters D to δD is determined using the average value of the constant b, which is equal to 0.0144.

$$\begin{aligned}\delta N&=\frac{6\times 0.0144\,\delta D}{2430\,\pi\,D^3}=\frac{1.132\times 10^{-5}}{D^3}\,\delta D\\&=N_T\frac{k}{D^3}\,\delta D=N_T\,n(D)\,\delta D\end{aligned} \tag{A5}$$

where N_T is the total number of suspended particles per unit volume of air and n(D) is the probability density function (or number degree distribution) and is obtained by:

$$\begin{aligned}&n(D)=\frac{a'}{D^3}\quad\text{and}\\&a'\equiv\frac{1.132\times 10^{-5}}{N_t}=\frac{2\,D_O^2\,D_h^2}{D_h^2-D_o^2}\end{aligned} \tag{A6}$$

Measurements indicate that dust particles have a minimum diameter ranging from 0.2 to 18 μm, with an average of 11 μm. The maximum diameter falls between 68 and 300 μm, with an average of 75.3 μm. Based on these averages, the constant "a'" was calculated to be 247 μm using equation (9). For Sudan dust samples, the average diameter of a' is $2.48\text{x}10^{10}$ when D measured in meters.

$$n(D)=\frac{2.48\times 10^{10}}{D^3} \tag{A7}$$